Electrochemical and Solid-State Letters, **15** (6) K49-K52 (2012)
1099-0062/2012/15(6)/K49/4/$28.00 © The Electrochemical Society

Synthesis and Characterization of Orthorhombic Sb_2O_4 Nanowire Prepared by Heating Sb_2S_3 Powder

Hyoun Woo Kim,[a] Han Gil Na,[a] Joonho Bae,[b] Ju Chan Yang,[a] Sung Soo Kim,[c] Hyeonsik Cheong,[c] and Doo Young Kim[d,z]

[a]*Division of Materials Science and Engineering, Hanyang University, Seoul 133-791, Korea*
[b]*School of Materials Science and Engineering, Georgia Institute of Technology, Atlanta, Georgia 30332-0245, USA*
[c]*Department of Physics, Sogang University, Seoul 121-742, Korea*
[d]*Department of Chemistry, University of Kentucky, Lexington, Kentucky 40506-0055, USA*

Orthorhombic, α- phase, Sb_2O_4 nanowire was fabricated by heating Sb_2S_3 powder. At 500°C, the grown product had the morphology of nanowire with an average diameter of ∼100 nm. At 600°C, it became a continuous film with nodular morphology. The structure, crystallinity, and phase-purity of the nanowire were investigated using X-ray diffraction spectroscopy, high-resolution transmission electron microscopy, and selected-area electron diffraction. These measurements, combined with those obtained using X-ray photoelectron, Raman, and photoluminescence spectroscopy, indicate that the as-grown nanowires were crystalline with an orthorhombic α-Sb_2O_4 structure. This study confirmed that thermal evaporation of the Sb_2S_3 precursor is a viable and simple approach to produce nanostructured α–Sb_2O_4 materials selectively.
 [DOI: 10.1149/2.028206esl]

Manuscript submitted January 16, 2012; revised manuscript received March 21, 2012. Published April 10, 2012.

One-dimensional (1D), nanostructured materials (nanotubes, nanobelts, nanowires, and nanoribbons) have attracted significant attention because of their unique and desirable physical, optical, electronic, and magnetic properties. Extensive research efforts have been made with the goal of optimizing the performance of these nanostructured materials for a variety of applications, such as sensing, nanodevices, and catalysis.[1–4] Accordingly, considerable efforts have been made to fabricate various types of nanowires.[5–11]

A few different antimony oxides are known to exist at 1 atm and temperatures up to 1250°C, e.g., Sb_2O_3, Sb_2O_4, Sb_2O_5, and Sb_6O_{13}.[12] Antimony trioxide (Sb_2O_3) has been used extensively in various applications, e.g., as a retardant, filler, catalyst, and in optical materials.[13–16] Sb_2O_3 is an interesting semiconducting material with unique optical and optoelectronic properties, and it also has remarkable magnetic properties.[17–19] Antimony pentoxide (Sb_2O_5) has been used extensively as a flame retardant due to its stability at very high temperatures, covering power, and transparency.[13,21] Also, Sb_2O_5 possesses a high refractive index and high abrasive resistance, so it is used widely as an optical material.[21] In recent years, nanostructured Sb_2O_3 and Sb_2O_5 materials have been synthesized by various methods,[20–27] and they have exhibited some interesting properties that usually are not found in bulk materials (e.g., transition from indirect to direct band-gap).[26]

Previous studies related to Sb_2O_4, especially nanostructrured Sb_2O_4, are marginal, compared to the available literature references on Sb_2O_3 and Sb_2O_5 materials. Catalytic activity of α-Sb_2O_4 and its applications in optics and electronics were previously reported.[28,29] Jansen et al. (YEAR) synthesized bulk Sb_2O_4 by heating Sb_2O_3 powder using oxygen flow, and they studied the conversion of α-Sb_2O_4 to β-Sb_2O_4 at high pressure and high temperature.[12] Other groups have reported the fabrication of Sb_2O_4 nanorods by either the mixture of Sb_2O_3 and Sb_2O_5 powders or the hydrothermal approach.[28,30,31]

In this paper, we report on the successful growth of pure Sb_2O_4 nanowires without using templates and without producing other antimony oxides. The detailed structure, phase, chemical composition, and the photoluminescence property of as-grown Sb_2O_4 nanowires are discussed.

Experimental

Antimony oxide nanowires were grown in a quartz tube by heating the source material of Sb_2S_3 powder. The detailed experimental procedure for the growth was described elsewhere.[32] First, a thin, gold film (3 nm thick) was deposited on a silicon substrate using a turbo sputter coater (Emitech K575X, Emitech, Ltd., Ashford, Kent, UK). Antimony sulfide (Sb_2S_3, Aldrich) powder was used as the source material for the growth and it was placed in the ceramic boat at the center of the quartz tube. Then, a Au-coated Si substrate was placed 10 mm above the antimony sulfide powder. During the growth, Ar and O_2 gases flowed with a total pressure of 2 Torr. The partial pressures of O_2 and Ar were maintained at 3% and 97% of total pressure, respectively. Various temperatures were used during the growth of the nanowires, i.e., 400°C, 500°C, and 600°C, and the growth period was 1 h. After the growth, the chamber was cooled, and the sample was removed for analysis.

The morphology, crystallinity, and phase of as-grown samples were investigated using glancing angle (0.5°) X-ray diffraction (XRD, X'pert MPD-Philips with Cu$K\alpha_1$ radiation), scanning electron microscopy (SEM, Hitachi S-4200), and transmission electron microscopy (TEM, Philips CM-200) with energy-dispersive X-ray (EDX) spectroscopy and the selected-area electron diffraction (SAED) attached. Carbon-coated nickel grids were used as the sample holders.

X-ray photoelectron spectroscopy (XPS) was used to investigate the valence state and chemical composition of the nanowires that were grown. The XPS system is a Kratos Axis-165 equipped with both Al/Mg twin-anode and monochromated Al X-ray guns. Raman spectroscopy was used to examine the complex vibrational states of the nanowires. Raman spectra were collected in a backscattered collection geometry using a 100-mW argon ion laser (Melles Griot CW) at the excitation wavelength of 514.5 nm. Furthermore, room temperature photoluminescence (PL) measurements of the Sb_2O_4 nanowires were performed. A 325nm line from a He-Cd laser (Kimon, Japan) was used for the excitation for PL measurements.

Results and Discussion

Antimony oxide nanowires were grown by heating Sb_2S_3 powder, and the morphology, crystallinity, and phase of the as-grown products were investigated as a function of temperature. Figure 1 presents the top-view SEM images and corresponding XRD spectra. At 400°C (Fig. 1a), a SEM image revealed agglomerated particles, and the corresponding XRD spectrum indicated that these particles were from a pre-deposited Au layer. At this temperature, there was no indication of sample growth, other than Au particle agglomeration. When the temperature was raised to 500°C (Fig. 1b), dense 1-D nanostructures were observed with an average diameter of approximately 100 nm. The XRD spectrum indicated that these nanowires can be well indexed

[z]E-mail: dooyoung.kim@uky.edu

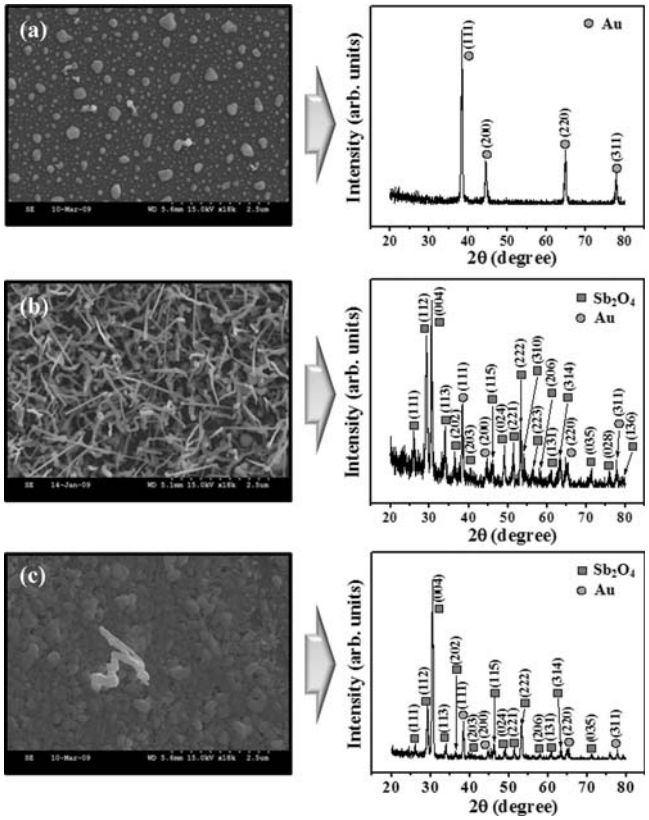

Figure 1. SEM images (left) and XRD patterns (right) of as-synthesized product grown at (a) 400°C, (a) 500°C, and (c) 600°C.

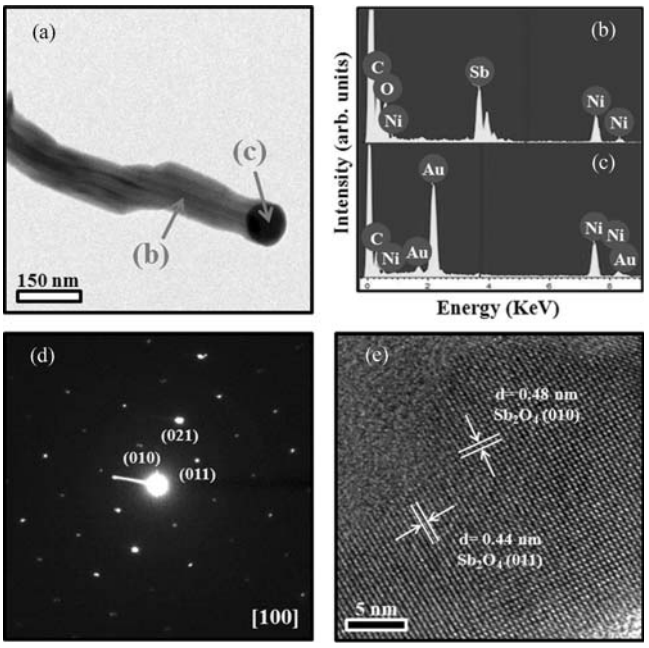

Figure 2. (a) Low-magnification TEM image. (b,c) EDX spectra from the region indicated by (b) Arrow 1 and (c) Arrow 2 in (a). Ni signals are from background scattering off the TEM copper grid. (d) Associated SAED pattern. (e) Lattice-resolved HRTEM image.

to the orthorhombic α-Sb_2O_4 structure (Sb(III)Sb(V)O_4) with lattice constants of a = 5.44 Å, b = 4.80 Å, and c = 11.78 Å, which are in excellent agreement with literature data (JCPDS: 11-0694).[33] Therefore, phase-pure α-Sb_2O_4 nanowires were fabricated successfully at a growth temperature of 500°C. When temperature was increased to 600°C (Fig. 1c), the morphology changed to 2-dimensional, nodular structures by agglomeration. Despite the significant change in morphology, the corresponding XRD characteristics were similar to those at 500°C, indicating that the phase is still orthorhombic α-Sb_2O_4.

The morphology and structure of the as-grown sample were investigated further by transmission electron microscopy (TEM). Figure 2a shows a representative, low-magnification, TEM image of a single α-Sb_2O_4 nanowire, exhibiting a dark nanoparticle attached to the tip. This TEM image shows that the diameter of the nanowire is similar to that of the dark nanoparticle (approximately 100 nm). In order to determine the chemical composition of an individual nanowire, energy-dispersive X-ray spectra (EDX) were measured on the wire stem (Arrow 1 in Fig. 2a) and on the wire tip (Arrow 2 in Fig. 2a). The position-dependent EDX patterns indicated that the nanowire stem consists of Sb and O (Fig. 2b), whereas the nanowire tip was composed mainly of Au (Fig. 2c). Additional C and Ni signals in the EDX spectra were generated from the carbon support and the Ni mesh of the grid, respectively. Figure 2d shows an associated, selected-area, electron-diffraction (SAED) pattern, which can be indexed for the [111] zone axis of an α-Sb_2O_4 nanowire. The well-defined SAED pattern indicated that the structure of the α-Sb_2O_4 nanowire is single-crystalline. Figure 2e is a representative, high-resolution TEM (HRTEM) image obtained on the stem of a single nanowire. Two crystal planes were clearly visible with the spacing of 0.44 nm and 0.48 nm, corresponding to the (011) and (010) planes of the orthorhombic α-Sb_2O_4 structure, respectively.[12,30] The HRTEM image indicated that the individual antimony oxide nanowires were single-crystalline and that they were surrounded by a thin amorphous layer (left, upper side of Figure 2e).

Generally, two mechanisms are accepted for explaining the growth of 1D nanostructures, i.e., vapor-liquid-solid (VLS) and vapor-solid (VS) mechanisms. In the present work, the presence of Au nanoparticles at the ends of the nanowires suggested that the growth occurred by the VLS mechanism. Therefore, the growth of Sb_2O_4 nanowires may proceed according to the following steps. In the first step, the source material, i.e., Sb_2S_3 powder, is evaporated and decomposed according to the following reaction:

$$Sb_2S_3\,(g) \rightarrow 2Sb + 3S(g)$$

In the second step, Sb vapor is transported to form the liquid-phase droplets consisting of Au/Sb/O on the substrate. Oxygen in the droplet is provided from the carrier gas. In the third step, as the droplets or nanoparticles become supersaturated, the growth of Sb_2O_4 nanowires is initiated. In the fourth step, by continuously dissolving Sb and O into the nanoparticles, Sb_2O_4 nanowires may subsequently grow. The formation of Au catalytic particle and the nanowire growth are illustrated in Figure 3. The favorable phase of antimony oxide (Sb_2O_3,

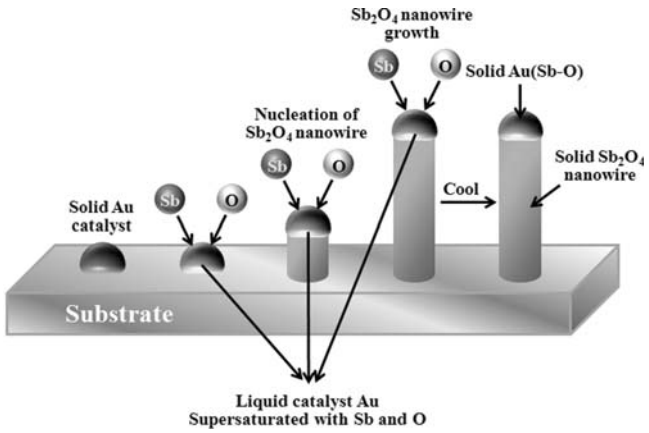

Figure 3. Schematic illustration of VLS process for Sb_2O_4 nanowire growth.

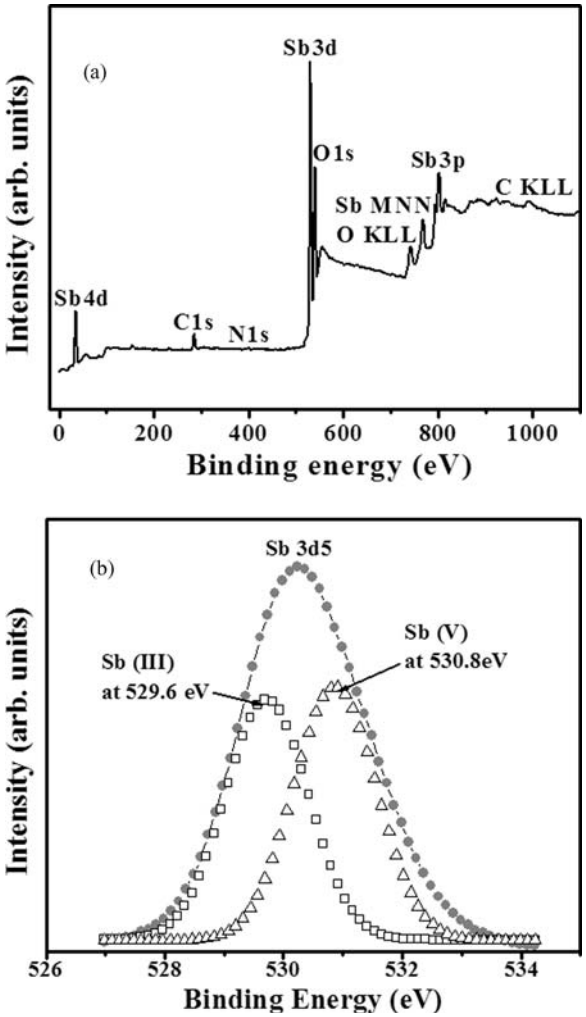

Figure 4. (a) XPS spectra of Sb_2O_4 nanowires grown at 500°C and (b) a peak fitting analysis with two Gaussian peaks centered at 529.6 and 530.8 eV, corresponding to Sb(III) and Sb(V), respectively.

Sb_2O_4, Sb_2O_5) to be formed at certain temperature is determined by thermodynamics, kinetics and the content of oxygen.[34] Apparently, the formation of the Sb_2O_4 phase is preferred in the present synthetic process.

The antimony in both Sb_2O_3 and Sb_2O_5 compounds has pure valence states, i.e., III and V, respectively, but the antimony in Sb_2O_4 has mixed valence states.[28,30] In order to further examine the chemical composition of the as-grown nanowires and the valence states of Sb, X-ray photoelectron spectroscopic measurement (XPS) was conducted. Fig. 4 shows a representative XPS spectrum (Fig. 4a) of the as-grown nanowires. Peaks for antimony and oxygen are clearly resolved in the spectrum. The peak for the Sb $3d_{5/2}$ orbital is centered at 530.2 eV and is slightly asymmetric due to the mixed valence state of Sb. As shown in Fig. 4b, this peak was analyzed by a curve fitting of two Gaussian peaks. The two Gaussian peaks that were analyzed were centered at 529.6 and 530.8 eV, corresponding to the binding energies of the $3d_{5/2}$ orbitals of Sb (III) and Sb (V), respectively. They had similar peak areas, reflecting the equal fraction of Sb (III) and Sb (V) participating in Sb-O chemical bonds. This XPS result confirmed that the nanowire has a chemical structure that is made up of the combination of Sb(III)-O and Sb(V)-O.

As discussed above, the antimony in the as-grown antimony oxide nanowires had an average oxidation state of Sb(IV) due to the equal amount of the Sb(III) and Sb(V) oxidation states. An Sb(III) atom and four surrounding oxygen atoms form a tetragonal polyhedral, whereas

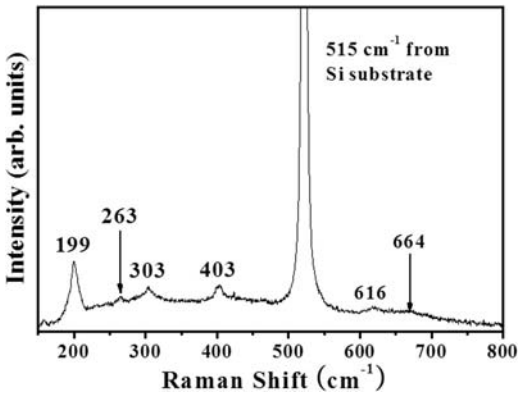

Figure 5. Representative Raman spectrum of as-grown antimony oxide nanowires grown at 500°C. The line for excitation was 514.5 nm from Ar-ion laser.

an Sb(V) atom and six oxygen atoms form an octahedral structure. Due to the mixed oxidation states of antimony in orthorhombic α- Sb_2O_4, it displays distinctive and complicated vibration modes. Figure 5 is the representative Raman spectrum of the as-grown antimony oxide nanowires grown at 500°C. The Raman peaks are evident at 199, 263, 303, 403, 515, 616, and 664 cm^{-1}, which indicated good agreement with values that have been reported in the literature for bulk α-Sb_2O_4 and α-Sb_2O_4 nanowires.[30,35] The most intense peak at 515 cm^{-1} is from the first order phonon of the Si substrate, not from antimony oxide. The peaks at 199 and 263 cm^{-1} are from the vibration of O-Sb(III)-O,[29] and the peak at 403 cm^{-1} was attributed to the stretching of the Sb(III)-O-Sb(V).[29,32] Broad and weak peaks at about 616 and 664 cm^{-1} can be attributed to the vibration of O-Sb(V)-O in the octahedron.[30,35] The peaks at 616 and 664 cm^{-1} were fairly weak, because these peaks are normally IR-active and Raman-forbidden modes.[35]

The photoluminescence (PL) spectra of the α-Sb_2O_4 nanowires grown at 500°C are shown in Figure 6. For the PL spectrum, the 325-nm line was used for the excitation. A peak-fitting analysis with multiple Gaussian functions revealed that the PL spectrum consists mainly of two bands, i.e., one centered at 439 nm (in the blue region) and the other at 525 nm (in the green region). In polycrystalline metallic oxides, oxygen-related vacancies and defects are known to be the most common emitting sites. These defect sites accept the energy from the photo-excitation via Forster-resonance energy transfer (FRET) and emit at longer wavelengths than the original excitation.[36] The more defect sites there are in a metal oxide, the more efficient FRET is and the stronger the defect emissions are. A similar photoluminescence (PL) spectrum was reported by Ji et al., who reported the absorption and emission spectra of Sb_2O_4 nanorods that were prepared

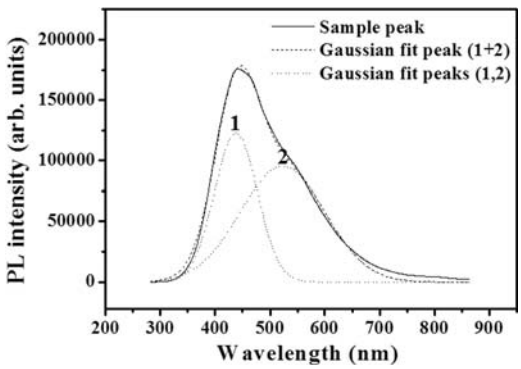

Figure 6. PL emission spectra of the Sb_2O_4 nanowires grown at 500°C. The laser excitation was at 325 nm.

via the solvothermal process.[28] In this work, the absorption spectrum of Sb_2O_4 nanorods showed two peaks, both at around 365 nm, which were attributed to the excitation of two different valence states (III, V) of antimony. The emission peak was centered at 450 nm, which is similar to our emission spectrum. A large shift between the absorption and emission peaks was indicative of the occurrence of energy transfer from the originally excited site to the defect sites. Also, it has been reported that the intensity of green emission, which peaked around 515 nm, was increased significantly by doping Sb to $PbWO_4$ single crystals, in which the doped Sb takes the form of Sb^{3+} and/or Sb^{5+}.[37]

Conclusion

In summary, we synthesized α-Sb_2O_4 nanowires at the temperatures of 500 and 600°C on Si substrates on which Au was predeposited. The structure, crystallinity, and phase purity of the as-grown nanowires were investigated by XRD, TEM, SAED, XPS, and Raman spectroscopy. All these investigations consistently showed that the nanowires were crystalline with an orthorhombic Sb_2O_4 structure. The presence of Au-containing nanoparticles at the tips of the nanowires suggested that the growth mechanism of Sb_2O_4 nanowires mainly involved a VLS-type process. The PL measurement with the Gaussian fitting showed that apparent visible light emission bands were centered at 439 nm and 525 nm. This study showed that the thermal evaporation of Sb_2S_3 precursor powder is a viable approach for selectively synthesizing nanostructured α–Sb_2O_4 at 500–600°C.

Acknowledgment

This research is supported by the University of Kentucky faculty start-up grant.

References

1. G. Fasol, *Science*, **280**, 545 (1998).
2. Z. Zhong, D. Wang, Y. Cui, M. Bockrath, and C. M. Lieber, *Science*, **302**, 1377 (2003).
3. X. Duan, C. Niu, V. Sahi, J. Chen, J. Parce, S. Empedocles, and J. Goldman *Nature*, **425**, 274 (2003).
4. Z. W. Pan, Z. R. Dai, and Z. L. Wang, *Science*, **291**, 1947 (2001).
5. L. D. Hicks and M. S. Dresselhaus, *Phys. Rev. B*, **47**, 16631 (1993).
6. A. P. Alivisatos *Science*, **271**, 933 (1996).
7. J. T. Hu, T. W. Odom, and C. M. Lieber, *Acc. Chem. Res.*, **32**, 435 (1999).
8. J. D. Holms, K. P. Johnston, R. C. Doty, and B. A. Korgel, *Science*, **287**, 1471 (2000).
9. M. H. Huang, S. Mao, H. Feick, H. Q. Yan, Y. Y. Wu, H. Kind, E. Weber, R. Russo, and P. Yang, *Science*, **292**, 1897 (2001).
10. Z. R. Dai, Z. W. Pan, and Z. L. Wang, *Adv. Funct. Mater.*, **13**, 9 (2003).
11. P. Yang, H. Yan, S. Mao, R. Russo, J. Johnson, R. Saykally, N. Morris, J. Pham, R. He, and H.-J. Choi, *Adv. Funct. Mater.*, **12**, 323 (2002).
12. D. Orosel, P. Balog, H. Liu, J. Qian, and M. Jansen, *J. Solid State Chem.*, **178**, 2602 (2005).
13. H. Sato, K. Kondo, S. Tsuge, H. Ohtani, and N. Sato, *Polym. Degrad. Stab.*, **62**, 41 (1998).
14. J. Spengler, F. Anderle, E. Bosch, R. K. Grasselli, B. Pillep, P. Behrens, O. B. Lapina, A. A. Shubin, H. J. Eberle, and H. Knozinger, *J. Phys. Chem. B*, **105**, 10772 (2001).
15. H. C. Liu, H. Imoto, T. Shido, and Y. Iwasawa, *J. Catal.*, **200**, 69 (2001).
16. B. Duh, *Polymer*, **43**, 3147 (2002).
17. H. H. Liu and Y. Iwasawa, *J. Phys. Chem. B*, **106**, 2319 (2002).
18. B. V. Raghavaiah, R. D. Krishna, and N. Veeraiah, *J. Magn. Magn. Mater.*, **284**, 363 (2004).
19. M. S. Reddy, G. M. Krishna, and N. Veeraiah, *J. Phys. Chem. Solids*, **67**, 789 (2006).
20. G. K. Semin and A. A. Boguslavsky, *Chem. Phys. Lett.*, **251**, 250 (1996).
21. H.-M. Xiong, J.-S. Chen, and D.-M. Li, *J. Mater. Chem.*, **13**, 1994 (2003).
22. Z. Deng, F. Tang, D. Chen, X. Meng, L. Cao, and B. Zou, *J. Phys. Chem. B*, **110**, 18225 (2006).
23. L. Guo, Z. Wu, T. Liu, W. Wang, and H. Zhu, *Chem. Phys. Lett.*, **318**, 49 (2000).
24. B. C. Satishkumar, A. Govindaraj, M. Nath, and C. N. R. Rao, *J. Mater. Chem.*, **10**, 2115 (2000).
25. C. Ye, G. Meng, L. Zhang, G. Wang, and Y. Wang, *Chem. Phys. Lett.*, **363**, 34 (2002).
26. Z. Deng, D. Chen, F. Tang, X. Meng, J. Ren, and L. Zhang, *J. Phys. Chem. C*, **111**, 5325 (2007).
27. X. Y. Chen, H. S. Huh, and S. W. Lee, *J. Solid State Chem.*, **181**, 2127 (2008).
28. T. Ji, M. Tang, L. Guo, X. Qi, Q. Yang, and H. Xu, *Solid State Commun.*, **133**, 765 (2005).
29. Y. Huang and P. Ruiz, *Appl. Surf. Sci.*, **252**, 7849 (2006).
30. G. Ren, C. Wang, J. Xia, J. Liu, and H. Zhong, *Mater. Lett.*, **63**, 605 (2009).
31. Z. J. Zhang and X. Y. Chen, *J. Phys. Chem. Solids*, **70**, 1121 (2009).
32. H. W. Kim, N. H. Kim, J. H. Myung, and S. H. Shim, *Phys. Stat. Sol.(a)*, **202**, 1758 (2005).
33. L. Labachev, *High Temp. High Press.*, **6**, 687 (1974), www.hthpweb.com/.
34. H. S. Chin, K. Y. Cheong, and K. A. Razak, *J. Mater. Sci.*, **45**, 5993 (2010).
35. G. Mestl, P. Ruiz, B. Delmon, and H. Knözinger, *J. Phys. Chem.*, **98**, 11276 (1994).
36. W. R. Algar, D. Wegner, A. L. Huston, J. B. Blanco-Canosa, M. A. H. Stewart, A. Armstrong, P. E. Dawson, N. Hildebrandt, and I. L. Medintz, *J. Am. Chem. Soc.*, **124**(3), 1876 (2012).
37. Y. Chen, C. Shi, and G. Hu, *J. Appl. Phys.*, **87**, 1503 (2000).